

# Understanding the Early Stages of the Methanol-to-Olefin Conversion on H-SAPO-34

Weili Dai,<sup>†</sup> Chuanming Wang,<sup>‡</sup> Michael Dybala,<sup>§</sup> Guangjun Wu,<sup>†</sup> Naijia Guan,<sup>†</sup> Landong Li,<sup>\*,†</sup> Zaiku Xie,<sup>‡</sup> and Michael Hunger<sup>\*,§</sup>

<sup>†</sup>Key Laboratory of Advanced Energy Materials Chemistry of Ministry of Education, Collaborative Innovation Center of Chemical Science and Engineering (Tianjin), Nankai University, Tianjin 300071, China

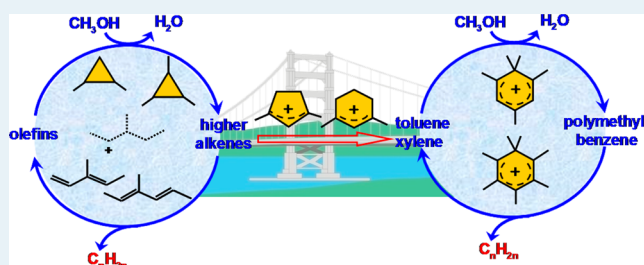
<sup>‡</sup>Shanghai Research Institute of Petrochemical Technology, SINOPEC, Shanghai 201208, P.R. China

<sup>§</sup>Institute of Chemical Technology, University of Stuttgart, 70550 Stuttgart, Germany

## S Supporting Information

**ABSTRACT:** Little is known on the early stages of the methanol-to-olefin (MTO) conversion over H-SAPO-34, before the steady-state with highly active polymethylbenzenium cations as most important intermediates is reached. In this work, the formation and evolution of carbenium ions during the early stages of the MTO conversion on a H-SAPO-34 model catalyst were clarified via <sup>1</sup>H MAS NMR and <sup>13</sup>C MAS NMR. Several initial species (i.e., three-ring compounds, dienes, polymethylcyclopentenyl, and polymethylcyclohexenyl cations) were, for the first time, directly verified during the MTO conversion. Their detailed evolution network was established from theoretical calculations. On the basis of these results, an olefin-based catalytic cycle is proposed to be the primary reaction pathway during the early stages of the MTO reaction over H-SAPO-34. After that, an aromatic-based cycle may be involved in the MTO conversion for long times on stream.

**KEYWORDS:** methanol-to-olefin conversion, H-SAPO-34, dual cycle mechanism, polymethylcyclopentenyl cations, polymethylcyclohexenyl cations, density functional theory calculation



## 1. INTRODUCTION

As an alternative process to obtain lower olefins, the methanol-to-olefin (MTO) conversion over microporous zeolite catalysts has attracted significant attention, since it was disclosed in 1977.<sup>1–6</sup> The MTO reaction is known as a complex reaction, and the understanding of its reaction mechanism is becoming a popular and challenging topic in heterogeneous catalysis recently. Among many controversial mechanisms, an indirect pathway (i.e., the hydrocarbon pool mechanism) is well accepted in the MTO conversion, consisting mainly of larger polyalkylaromatic molecules acting as a catalytic scaffold in the MTO conversion.<sup>7–11</sup> The importance of this indirect route for olefin formation for the future chemical industry has attracted extensive experimental and theoretical studies, focusing on the details of the hydrocarbon pool species, their formation, as well as their further reaction pathway. In the past years, a dual-cycle mechanism for the MTO conversion on zeolite catalysts has been intensively discussed, which consists of competitive olefin-based and aromatic-based cycles of methanol addition and a splitting off of light olefins.<sup>3,4,12–17</sup> Depending on the zeolitic pore system, different active hydrocarbon species are formed and dominate the MTO conversion, which strongly influences the product distribution.<sup>15–17</sup>

Recently, several types of carbenium ions involved in MTO conversion, especially in the aromatic-based cycle, have been

observed and confirmed as the active hydrocarbons in zeolite catalysts via <sup>13</sup>C NMR spectroscopy (e.g., polymethylcyclopentenyl cations on H-ZSM-5<sup>18</sup> and heptamethylbenzenium on H-beta<sup>19</sup> and H-SAPO-34<sup>20</sup>). However, no direct experimental clues have been reported toward the initial species evocating the well-accepted hydrocarbon pool in working MTO catalysts. Because the origination of first carbon–carbon bond from methanol is still not known,<sup>1,3</sup> knowledge on the roles of specific olefins and carbenium ions in early stages of MTO conversion would be most helpful for the understanding of the full MTO reaction mechanism.

Herein, we present novel insights on the hydrocarbon pool chemistry in the early stages of the MTO conversion on H-SAPO-34 zeolite from combined spectroscopic observations and theoretical calculations. Some key initial species (e.g., three-ring compounds, dienes, polymethylcyclopentenyl cations, polymethylcyclohexenyl cations, and polymethylbenzenium cations) were directly observed and confirmed by solid-state NMR spectroscopy under the real working conditions of MTO conversion. Among these species, trimethylcyclopropane and dienes were directly observed as precursors to produce

Received: October 13, 2014

Revised: November 24, 2014

Published: November 26, 2014

polymethylcyclopentenyl cations and polymethylcyclohexenyl cations. Dimethylcyclohexenyl cations, a new type of carbenium ions in MTO conversion, were simultaneously observed with polymethylcyclopentenyl cation for the first time. The evolution of these carbenium ions were in situ monitored by UV–vis spectroscopy, and their reactivity was investigated via a method consisting of ammonia loading, UV–vis,  $^1\text{H}$  and  $^{13}\text{C}$  MAS NMR spectroscopy. Furthermore, on the basis of the experimental observations, an olefin-based catalytic cycle during the initial stages of MTO conversion is applied and explored by density functional theory (DFT) calculations. After the formation of an aromatic hydrocarbon pool, an olefin-based cycle and an aromatic-based cycle run simultaneously for the MTO conversion.

## 2. EXPERIMENTAL SECTION

**2.1. Preparation and Characterization of the H-SAPO-34 Catalysts.** The H-SAPO-34 model catalyst with the  $n_{\text{Si}}/(n_{\text{Al}} + n_{\text{P}} + n_{\text{Si}})$  ratio of 0.10 was prepared following the procedure in our previous paper.<sup>21</sup> X-ray powder diffraction (XRD) patterns of the prepared samples were performed on a Bruker D8 instrument using Cu  $K\alpha$  radiation ( $\lambda = 1.5418 \text{ \AA}$ ). The morphology of the as-synthesized sample was determined with a JEOL-JSM7500 field emission scanning electron microscope (FESEM). The  $^1\text{H}$ ,  $^{27}\text{Al}$ ,  $^{29}\text{Si}$ , and  $^{31}\text{P}$  MAS NMR spectra of the calcined samples were recorded on Bruker Avance III 400WB spectrometer at resonance frequencies of 400.3, 104.3, 79.5, and 161.9 MHz, respectively. Sample spinning rates of 8 kHz for  $^1\text{H}$ ,  $^{27}\text{Al}$ , and  $^{31}\text{P}$  nuclei and of 4 kHz for  $^{29}\text{Si}$  MAS NMR spectroscopy and using the parameters described elsewhere.<sup>22</sup>

**2.2. MTO Conversion on the H-SAPO-34 Catalysts.** The MTO reaction was investigated in a fixed-bed reactor at atmospheric pressure as described in ref 22. During these experiments, 0.1 g of the SAPO-34 catalysts (sieve fraction, 0.25–0.5 mm) was placed in a stainless steel reactor (5 mm i.d.) and activated under flowing  $\text{N}_2$  at 450 °C for 1 h. After cooling to the desired reaction temperature,  $^{13}\text{C}$ -methanol was injected at a rate of 0.5 mL/h, corresponding to the weight hourly space velocity of  $\text{WHSV} = 4.0/\text{h}$ . The products were analyzed by an online gas chromatograph, HP5890/II, with flame ionization detector (FID) and a packed-column Porapak Q to separate the  $\text{C}_1$ – $\text{C}_8$  hydrocarbons. The temperature of the column was maintained at 40 °C for 15 min and then increased to 200 °C with a heating rate of 10 °C/min.<sup>22</sup> After MTO conversion, the methanol flow was switched off at the reaction temperature without stopping the carrier gas flow until the catalyst was cooled down. Subsequently, the catalyst samples studied by NMR spectroscopy were transferred from the fixed-bed reactor into gastight MAS NMR rotors with the protection of dry nitrogen gas to avoid contact with air.

**2.3. Characterization of Organic Species Formed in the H-SAPO-34 Catalysts.** The nature of organic compounds formed on the catalysts during the MTO reaction was in situ monitored by UV–vis spectroscopy as described in ref 21. The UV–vis spectra were recorded in the diffuse reflection mode in the range of 200–600 nm using an AvaSpec-2048 fiber optic spectrometer, an AvaLight-DH-S deuterium light source by Avantes, and a glass fiber reflection probe HPSUV1000A by Oxford Electronics. Before starting the MTO reaction, the glass fiber reflection probe was placed in the fixed-bed reactor on the top of the catalyst with a gap of ca. 1.0 mm. Reference UV–vis spectra of catalysts were recorded at reaction temperature prior to starting the methanol flow.<sup>21</sup>

The fate of Brønsted acid sites and of the organic species formed during the MTO conversion was characterized by means of  $^1\text{H}$  MAS NMR spectroscopy utilizing a Bruker Avance III 400WB spectrometer at the resonance frequency of 400.1 MHz, with  $\pi/2$  single pulse excitation, the repetition time of 10 s, the sample spinning rate of 8.0 kHz by a 4.0 mm MAS NMR probe, and using a 4.0 mm MAS NMR probe and the parameters described elsewhere.<sup>21</sup>

To confirm the organic species formed and occluded in the cages of SAPO-34 catalysts,  $^{13}\text{C}$  MAS NMR spectroscopy was also carried out on a Bruker Avance III 400WB spectrometer at a resonance frequency of 100.6 MHz, with  $\pi/2$  pulse excitation, a repetition time of 20 s, and a sample spinning rate of 12.0 kHz.<sup>21</sup>

**2.4. Computational Methods.** The H-SAPO-34 model catalyst was represented by a hexagonal cell consisting of 36T atoms and having one acid site at O2 position (see Figure S1). The lattice constants are  $a = b = 13.90 \text{ \AA}$ ,  $c = 15.11 \text{ \AA}$ .<sup>23</sup> All density functional theory (DFT) calculations were carried out using the GPAW package and a real-space grid implementation of the projector augmented-wave method.<sup>24,25</sup> The grid spacing in the real-space was 0.20 Å. The sampling of the Brillouin zone was made with a  $\Gamma$  point only. The Bayesian error estimation functional with van der Waals correlation (BEEF-vdW) was employed.<sup>24,26</sup> The climbing image nudged elastic band (CI-NEB) method was used to locate all the transition states.<sup>27,28</sup> A force threshold of 0.03 eV/Å was used in these calculations.

## 3. RESULTS AND DISCUSSION

**3.1. Physico-Chemical Properties of the H-SAPO-34 Catalysts.** SEM micrograph and the XRD patterns of the as-synthesized H-SAPO-34 sample are shown in Figure 1. The

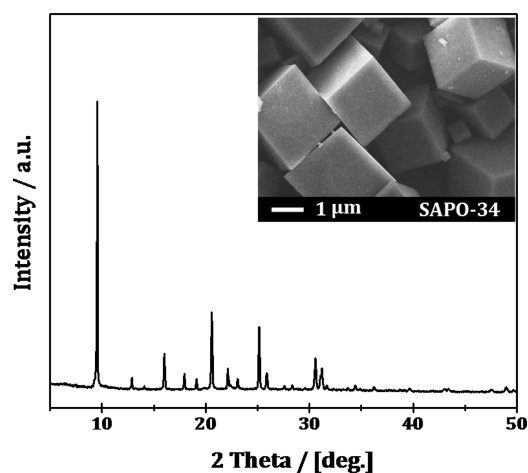


**Figure 1.** XRD pattern and SEM image of the as-synthesized SAPO-34 material.

typical XRD patterns corresponding to CHA-type framework structures of the as-synthesized sample, indicating that well-crystallized H-SAPO-34 sample without any impurity phases was obtained.<sup>29</sup> The SEM picture of the as-synthesized sample in the inset of Figure 1 exhibits typical cubical shape of H-SAPO-34 zeolite and with the average crystal size of 2  $\mu\text{m}$ .

After calcination, the textual properties of the H-SAPO-34 catalyst were investigated by  $^1\text{H}$ ,  $^{27}\text{Al}$ ,  $^{29}\text{Si}$ , and  $^{31}\text{P}$  MAS NMR spectroscopy (Figure 2). The predominant  $^1\text{H}$  MAS NMR signal at 3.6 ppm is attributed to Si(OH)Al groups (i.e.,

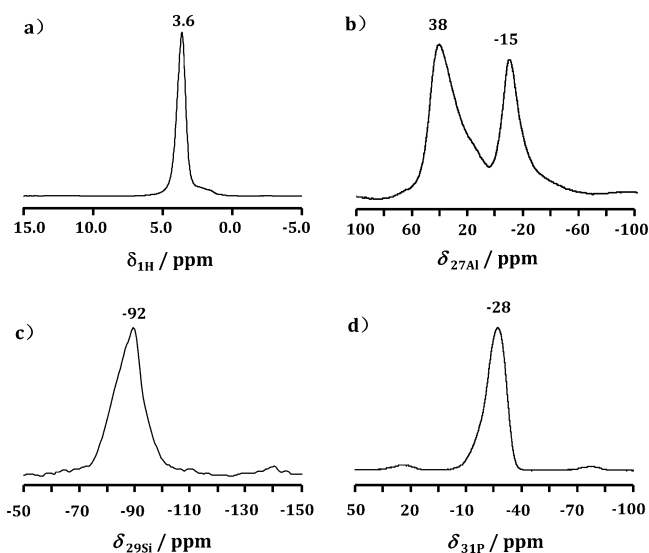
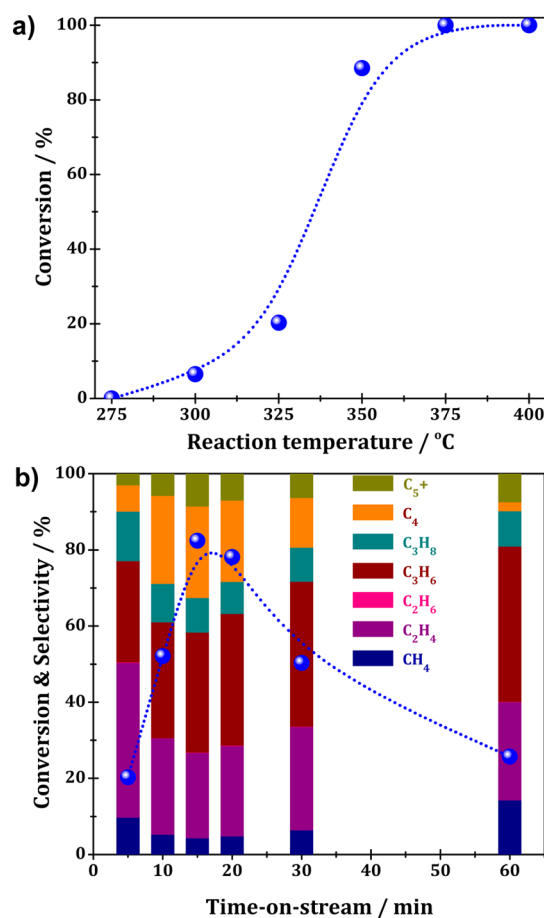


**Figure 2.**  $^1\text{H}$  (a),  $^{27}\text{Al}$  (b),  $^{29}\text{Si}$  (c), and  $^{31}\text{P}$  MAS NMR spectra (d) of the calcined H-SAPO-34 material recorded in the dehydrated state ( $^1\text{H}$ ) and upon rehydration ( $^{27}\text{Al}$ ,  $^{29}\text{Si}$ , and  $^{31}\text{P}$ ).

Brønsted acid sites).<sup>22</sup> The strong  $^{29}\text{Si}$  MAS NMR signal at  $-92$  ppm is assigned to  $\text{Si}(4\text{Al})$  species (i.e., tetrahedrally coordinated silicon atoms in the framework of SAPO-34 catalyst).<sup>30,31</sup> The dominant  $^{31}\text{P}$  NMR signal at  $-28$  ppm hints to the tetrahedrally coordinated framework phosphorus atoms.<sup>22,31</sup> The  $^{27}\text{Al}$  MAS NMR signal appearing at about  $38$  ppm is due to tetrahedrally coordinated framework aluminum atoms, whereas the signal occurring at about  $-15$  ppm is attributed to octahedrally coordinated aluminum atoms formed by an additional coordination of two water molecules to tetrahedrally coordinated framework aluminum atoms or by extra-framework aluminum species.<sup>21,32</sup> These results indicate that the framework of H-SAPO-34 material is well preserved and not damaged after calcination.

**3.2. Catalytic Performances of the H-SAPO-34 Catalysts during the MTO Conversion.** Reaction temperatures of  $275$ – $400$  °C were applied in the MTO conversion for a suitable identification, stabilization, and observation of the active hydrocarbon pool species. The catalytic activities of H-SAPO-34 catalysts during the MTO conversion at  $275$ – $400$  °C have been presented in Figure 3a. At  $275$  °C, no methanol conversion could be observed. When the reaction temperature increases to  $300$  °C, MTO reaction with a methanol conversion of  $6.5\%$  can be achieved. With the further increase of the reaction temperature, the methanol conversion gradually increases to  $100\%$ . Similar reaction conditions like described in the former reports of Kolboe and his co-workers,<sup>33</sup> the catalytic performance at the low temperature of  $325$  °C was focused thereafter to explore the hydrocarbons formed in the initial process of MTO conversion, and the catalytic activities of the H-SAPO-34 catalyst at different time-on-stream (TOS) are given in Figure 3b. At this reaction temperature, an induction period is obvious and a rapid deactivation of the catalyst can be observed, which starts already at TOS of  $20$  min.

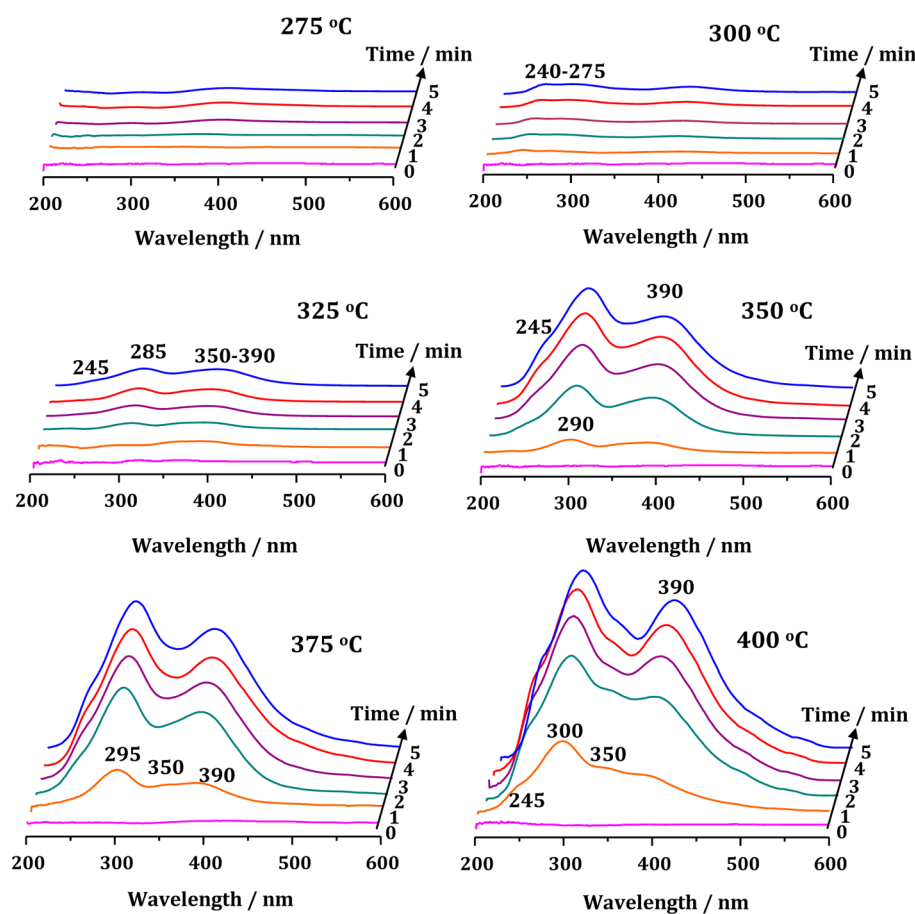
**3.3. In Situ and Ex Situ UV–vis Investigations of the MTO Conversion on the H-SAPO-34 Catalysts.** The organic species with UV–vis sensitivity formed in the MTO process were in situ monitored by UV–vis spectroscopy. The in situ UV–vis spectra recorded at different reaction temperatures with a TOS of  $5$  min are shown in Figure 4. At  $275$  °C, without



**Figure 3.** Methanol conversion (blue dots) on H-SAPO-34 at the time-on-stream of TOS =  $5$  min for different reaction temperatures (a) and methanol conversion (blue dots) and product selectivities (colored columns) obtained during the MTO conversion at  $325$  °C up to TOS =  $60$  min (b).

any methanol conversion, almost no UV–vis bands occurred. At higher reaction temperatures with significant MTO activity, several bands occurred in the range of  $240$ – $600$  nm, and their intensities gradually increased with increasing reaction temperature. Interestingly, the bands at  $240$ – $275$  nm are dominated in the UV–vis spectra at  $300$  °C. With a further increase in the reaction temperature ( $T \geq 325$  °C), new bands at  $330$ – $360$  and  $390$  nm occurred. According to previous studies, the bands at  $240$ ,  $275$ – $300$ ,  $330$ – $360$ , and approximately  $390$  nm are assigned to dienes (e.g., cyclopenta- and cyclohexadienes),<sup>34</sup> monoenylic carbenium ions (e.g., cyclopentenyl and cyclohexenyl cations)<sup>35</sup> or polyalkylaromatics,<sup>34</sup> dienylic carbenium ion,<sup>35</sup> and benzene-based carbenium ions,<sup>36,37</sup> respectively. The band positions of these species are directly related to the number of methyl groups, as reported by Olah et al.<sup>38</sup>

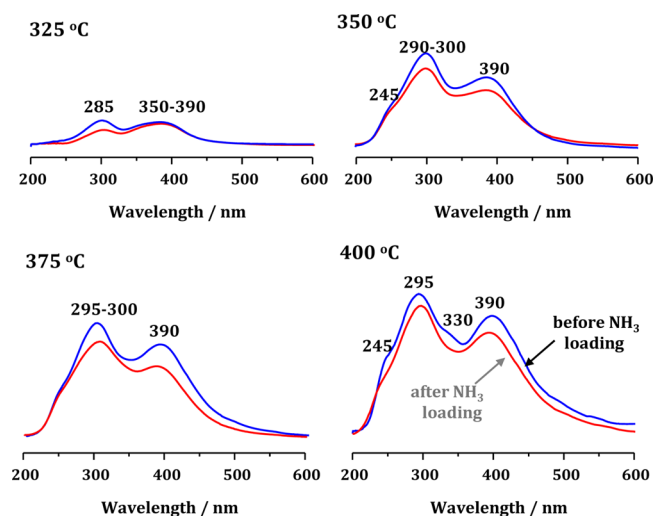
At  $325$  °C, the in situ UV–vis spectra with a longer TOS of up to  $60$  min recorded in the MTO conversion process on SAPO-34 catalyst are shown in Figure S2. Three broad bands occurred in the range of  $230$ – $600$  nm within the TOS of  $60$  min. With the progress of the MTO conversion, the band positions changed a little in the range of  $230$ – $248$ ,  $280$ – $300$  and  $350$ – $390$  nm, and this result means that the number of methyl groups in dienes, carbenium ions, and aromatics were changed with the increase of TOS. In addition, the intensities of the bands at  $280$ – $300$  nm were gradually higher than the bands



**Figure 4.** In situ UV–vis spectra recorded during the MTO conversion over H-SAPO-34 at reaction temperatures of 275–400 °C up to TOS of 5 min.

of 350–390 nm, indicating more polyalkylaromatics formed with the increase of TOS.

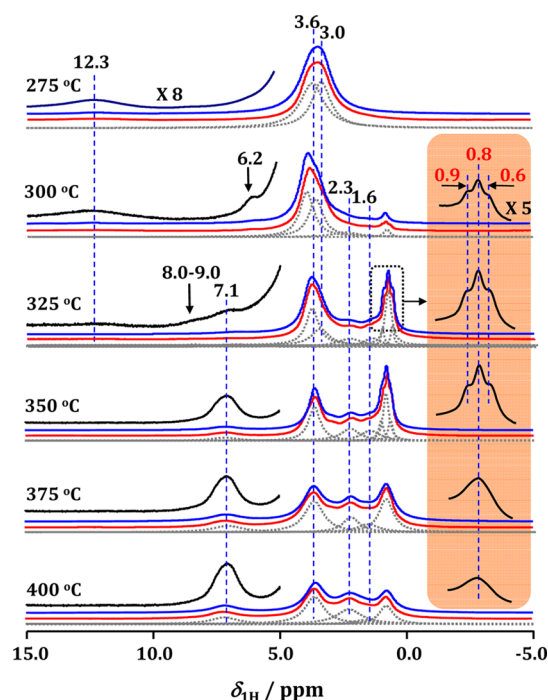
Previous studies have proved that ammonia as a strongly basic probe molecule can effectively evidence the presence of carbenium ions in order to study their reactivity. Bjorgen et al.<sup>37</sup> demonstrated that the UV–vis signal at about ca. 390 nm caused by hexamethylbenzenium cations in zeolite H-Beta immediately disappeared after the loading of ammonia. This finding hints that the hexamethylbenzenium ions can convert to the neutral moieties with the presence of ammonia. As a result, H-SAPO-34 catalysts gained after MTO reaction at different reaction temperatures in the present work were also studied by UV–vis spectroscopy in the ammonia-loaded state. The dominating UV–vis bands at about 300 and 390 nm of the used SAPO-34 catalysts (Figure 5, blue) significantly decreased upon loading of ammonia (Figure 5, red). This ammonia-induced decrease of the bands at about 300 and 390 nm indicates the presence of monoenylic carbenium ions (275–300 nm) (e.g., cyclopentenyl and cyclohexenyl cations) and benzene-based carbenium ions (390 nm).<sup>39</sup> It is interesting to note that only the signal at 270–300 nm decreased for the catalyst obtained at 325 °C after ammonia loading, while the signal at 390 nm nearly not changed. This indicates that the monoenylic carbenium ions (270–300 nm) are the dominant active species at lower reaction temperature ( $T \leq 325$  °C), and benzene-based carbenium ions together with monoenylic carbenium ions occurred simultaneously at higher reaction temperature ( $T \geq 350$  °C).



**Figure 5.** UV–vis spectra recorded during the MTO conversion over H-SAPO-34 at 325 °C and TOS = 5 min before (blue curves) and after loading of ammonia (red curves).

**3.4. <sup>1</sup>H MAS NMR Investigations of the Organic Species Formed over the H-SAPO-34 Catalysts during MTO Reaction.** After the in situ UV–vis measurements, MTO conversion was quenched and the used catalysts were transferred from the fixed-bed reactor into gastight MAS NMR rotors with the protection of dry nitrogen gas for <sup>1</sup>H and <sup>13</sup>C MAS NMR measurements.

Figure 6 shows the  $^1\text{H}$  MAS NMR spectra of the reacted H-SAPO-34 catalysts gained after TOS of 5 min at different



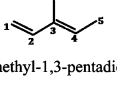
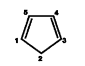


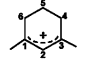
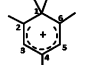


**Figure 6.**  $^1\text{H}$  MAS NMR spectra of H-SAPO-34 catalysts obtained after methanol conversion at different temperatures for TOS of 5 min. From top to bottom, the experimental spectra, the simulated spectra, and the signal components utilized for the simulation are shown.

reaction temperatures. At 275 °C, that is, without any methanol conversion (Figure 3), the dominant  $^1\text{H}$  MAS NMR signals at 3.6 and 3.0 ppm, characteristic for Brønsted acid sites<sup>35</sup> and methoxy groups ( $\text{CH}_3\text{O}-$ ),<sup>40</sup> respectively, can be observed. In addition, a broad and weak signal occurring at 12.3 ppm is induced by the hydroxyl protons involved in hydrogen bonds between methanol molecules and the zeolite framework.<sup>41</sup> At the reaction temperature of 300 °C, the methanol conversion increased to 6.5%, and new  $^1\text{H}$  MAS NMR signals appeared at  $\delta_{\text{H}} = 0.6-2.3$  and 6.2 ppm. The three weak signals at  $\delta_{\text{H}} = 0.6, 0.8,$  and  $0.9$  ppm indicate that organic three-ring alkanes, for example, dimethylcyclopropane ( $\delta_{\text{H}} = 0.40, 0.72, 0.93$  ppm)<sup>42</sup> and trimethylcyclopropane ( $\delta_{\text{H}} = 0.56, 0.89$  ppm),<sup>42,43</sup> are formed over H-SAPO-34 after a short reaction time. The signal at  $\delta_{\text{H}} = 6.2$  ppm can be attributed to dienes, such as cyclopentadiene ( $\delta_{\text{H}} = 2.80, 6.14, 6.22$  ppm),<sup>42</sup> and other long-chain pentadienes (Table 1).

At 325 °C, the methanol conversion increased to 20%, and more aliphatic compounds ( $\delta_{\text{H}} = 0.6-2.3$  ppm), including cyclopropanes, were formed. In addition, with the disappearance of dienes ( $\delta_{\text{H}} = 6.2$  ppm), a broad signal at  $\delta_{\text{H}} \cong 7$  ppm due to polymethylaromatics occurs.<sup>43</sup> At the low-field flank of the signal at  $\delta_{\text{H}} = 7.1$  ppm, a very broad signal at  $\delta_{\text{H}} = 8-9$  ppm appeared. Considering the low reaction temperature and the short reaction time, the assignment of this signal to polycyclic aromatics ( $\delta_{\text{H}} = 4.0-7.5$  ppm)<sup>42</sup> can be excluded. In addition, as the reaction was performed in a continuous-flow fixed-bed reactor, the water generated during the MTO conversion at high temperatures of 325–400 °C was immediately purged out by the flowing carrier gas ( $\text{N}_2$ ). For quenching the reaction, the methanol flow was switched off at

**Table 1. Schemes and Experimental  $^1\text{H}$  and  $^{13}\text{C}$  NMR Shifts of Neutral Hydrocarbons and Carbenium Ions Discussed in the Present Study**

Species	Chemical shifts $\delta_{\text{H}}$ and $\delta_{\text{C}}$ in ppm		References
	$^1\text{H}$ MAS NMR	$^{13}\text{C}$ MAS NMR	
 dimethylcyclopropane	0.72 (1, 2) 0.40 (3) 0.93 (4, 5)	16.0 (1, 2) 14.1 (3) 12.0 (4, 5)	38, 45
 trimethylcyclopropane	0.56 (1, 2, 3) 0.89 (4, 5, 6)	14.7 (1, 2, 3) 9.8 (4, 5, 6)	43, 48
 3-methyl-1,3-pentadiene	5.17 (1) 6.54 (2) 5.59 (4) 1.76 (5)	111.8 (1) 141.9 (2) 135.3 (3) 126.6 (4) 11.1 (5)	43, 48
 cyclopentadiene	6.14 (1, 3) 2.80 (2) 6.22 (4, 5)	132.8 (1, 3) 132.2 (4, 5) 41.6 (2)	43, 48
 1,3-dimethylcyclopentenyl cation	-8.30 (2) -4.00 (4, 5)	250.0 (1, 3) 147.0 (2) 48.0 (4, 5)	18, 44
 1,2,3-trimethylcyclopentenyl cation	3.46 (4, 5)	247.0 (1,3) 155.3 (2) 48 (4, 5)	44, 49
 1,3-dimethyl-2-cyclohexenyl cation	8.04 (2) 3.60 (4, 6) 2.60 (5)	226.6 (1, 3) 136.8 (2)	44
 1,1,2,4,6-pentamethylbenzium cation	/	58 (1) 206 (2, 6) 135 (3, 5) 190 (4)	19

the reaction temperature without stopping the carrier gas flow, while the catalyst was cooled down. By this method, the water generated during the MTO conversion was removed from the catalysts and it could not affect the  $^1\text{H}$  MAS NMR spectra. The presence of water would be negative for the spectral resolution and, therefore, had to be excluded. Moreover, as is shown in Figure 6 and Figure 7, the hydroxyl protons involved in hydrogen bonds between the unconverted methanol reactant and the framework of the zeolite give the broad signal at 12.3 ppm. Therefore, the signal at 8–9 ppm attributed to the hydrogen bond effect of water and methanol adsorption can also be excluded. According to the previous studies of Olah et al.,<sup>40</sup> the appearance of this signal may imply the formation of five-ring carbenium ions, such as 1,3-dimethyl-2-cyclopentenyl cations ( $\delta_{\text{H}} = 8.30, 4.00$  ppm),<sup>44</sup> or six-ring carbenium ions, such as 1,3-dimethyl-2-cyclohexenyl cations ( $\delta_{\text{H}} = 8.04, 3.60, 2.60$  ppm).<sup>44</sup> With a further increase of the reaction temperature ( $T \geq 350$  °C), more polymethylaromatics responsible for the signals at ca. 7 ppm were formed and overlapped the signals of carbenium ions at  $\delta_{\text{H}} = 8-9$  ppm. Simultaneously, the signals of three-ring compounds at  $\delta_{\text{H}} = 0.6-0.9$  ppm became weaker, implying the significantly lower number of three-ring alkanes at higher reaction temperature.

In order to investigate the fate of above-mentioned organic species and Brønsted acid sites during the MTO conversion, the  $^1\text{H}$  MAS NMR spectra of H-SAPO-34 sample gained after different TOS (0–60 min) at 325 °C before and after ammonia loading are shown in Figure 7. The dominated  $^1\text{H}$  MAS NMR

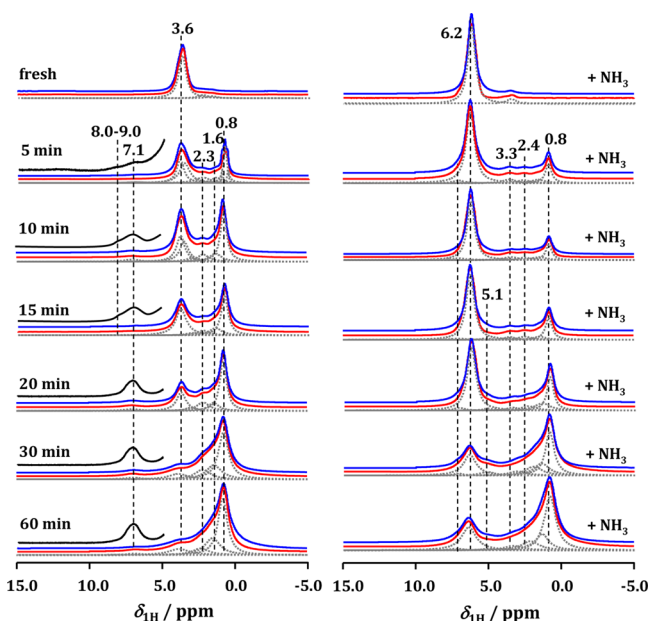


**Figure 7.**  $^1\text{H}$  MAS NMR spectra of H-SAPO-34 sample, obtained after different TOS at  $325\text{ }^\circ\text{C}$  and recorded before (left) and after (right) adsorption of ammonia. From top to bottom, the experimental spectra, the simulated spectra, and the signal components utilized for the simulation are shown.

signal at 3.6 ppm, due to the  $\text{Si}(\text{OH})\text{Al}$  groups, occurred in the fresh H-SAPO-34 catalyst (Figure 7, top, left). With the progress of MTO conversion, the number of  $\text{Si}(\text{OH})\text{Al}$  groups were gradually decreased, while polymethylaromatics at 7.1 ppm were gradually increased. Additionally, with the increase of TOS, the number of five-ring or six-ring carbenium ions reflected as the intensities of the signal at 8–9 ppm increased at

first, but then gradually decreased. After ammonia loading, a new signal at  $\delta_{1\text{H}} = 6.2$  ppm (Figure 7, top, right) occurs, which is attributed to protonation of the probe molecules, caused by accessible  $\text{Si}(\text{OH})\text{Al}$  groups, leading to the formation of ammonium ions.<sup>39,45</sup> For the catalyst obtained after TOS=15 min, an additional signal at  $\delta_{1\text{H}} = 5.1$  ppm occurred in the ammonium-loaded sample. According to our previous study, this signal is attributed to phenylammonium ions, formed by the reaction of ammonia with benzene-based carbenium ions.<sup>39</sup> With the increase of TOS, the number of benzene-type carbenium ions reflected as the intensities of the signal at 5.1 ppm increased at first, but then gradually decreased.

**3.5.  $^{13}\text{C}$  MAS NMR Investigations of the Organic Species Formed over the H-SAPO-34 Catalysts during MTO Reaction.** To further confirm the nature of the hydrocarbons formed during the initial process of the MTO reaction over the H-SAPO-34 catalyst,  $^{13}\text{C}$  MAS NMR measurements were also performed. Figure 8 exhibits the  $^{13}\text{C}$  MAS NMR spectra of the H-SAPO-34 catalysts after TOS = 5 min at different temperatures. Consistent with observations made by  $^1\text{H}$  MAS NMR spectroscopy (see Figure 6), the adsorbed methanol ( $\delta_{13\text{C}} = 50$  ppm),<sup>46</sup> DME ( $\delta_{13\text{C}} = 60$  ppm),<sup>46</sup> and surface methoxy species ( $\delta_{13\text{C}} = 56$  ppm)<sup>46</sup> are observed as predominant species occluded in the H-SAPO-34 catalyst after MTO conversion at  $275\text{ }^\circ\text{C}$  (Figure 8, top). After MTO conversion at  $300\text{ }^\circ\text{C}$ , in addition to the above-mentioned signals, some new peaks appear, even with low intensity, at 9–45 ppm and 120–125 ppm, attributed to the carbon atoms of alkyl groups and olefinic as well as aromatic compounds, respectively, can also be observed.<sup>39,47</sup> Moreover, consistent with observations made by  $^1\text{H}$  MAS NMR spectroscopy (see Figure 6), organic three-ring compounds, e.g., dimethylcyclopropane ( $\delta_{13\text{C}} = 12.00, 14.10, \text{ and } 16.0$

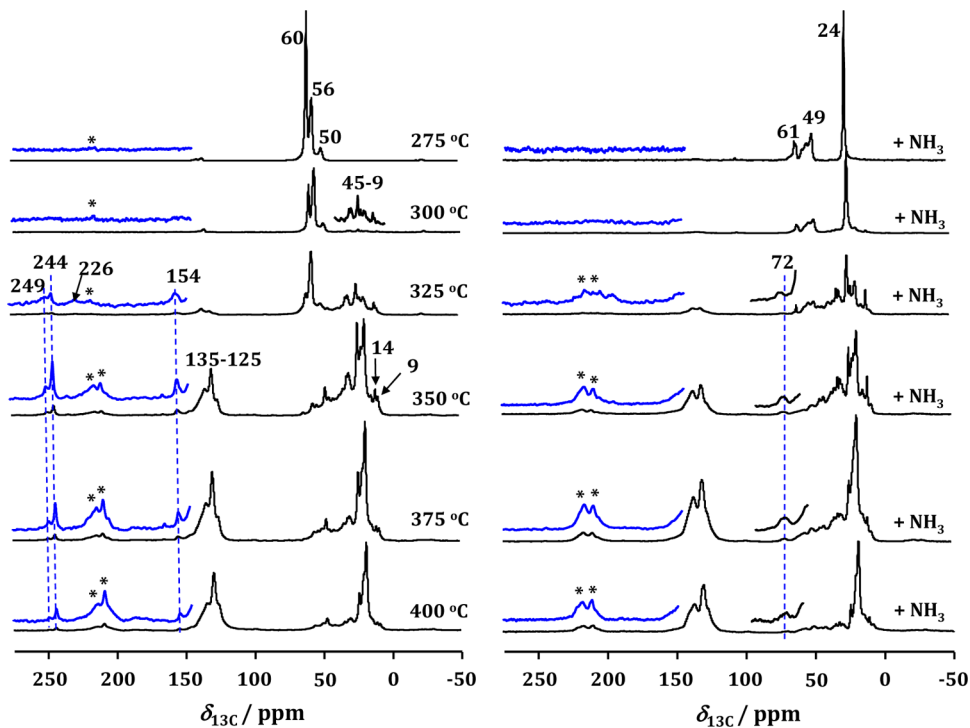


**Figure 8.**  $^{13}\text{C}$  MAS NMR spectra of used H-SAPO-34 catalysts obtained after MTO conversion at different temperatures for TOS of 5 min and recorded before (left) and after ammonia loading (right).

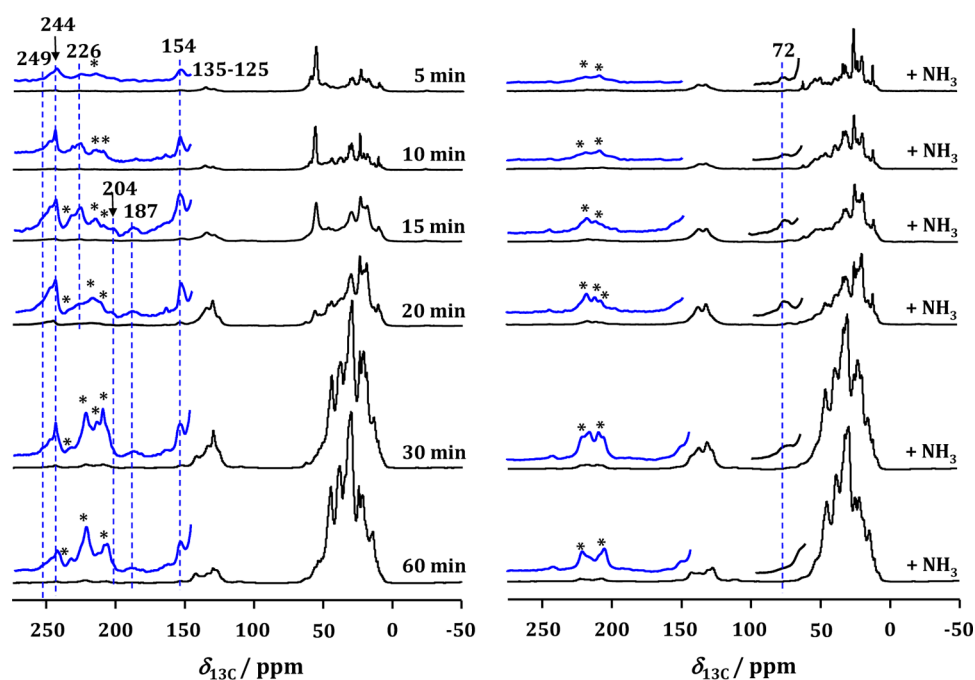


**Figure 9.**  $^{13}\text{C}$  MAS NMR spectra of used H-SAPO-34 catalysts obtained after MTO conversion at  $325\text{ }^\circ\text{C}$  for different TOS, recorded before (left) and after ammonia loading (right).

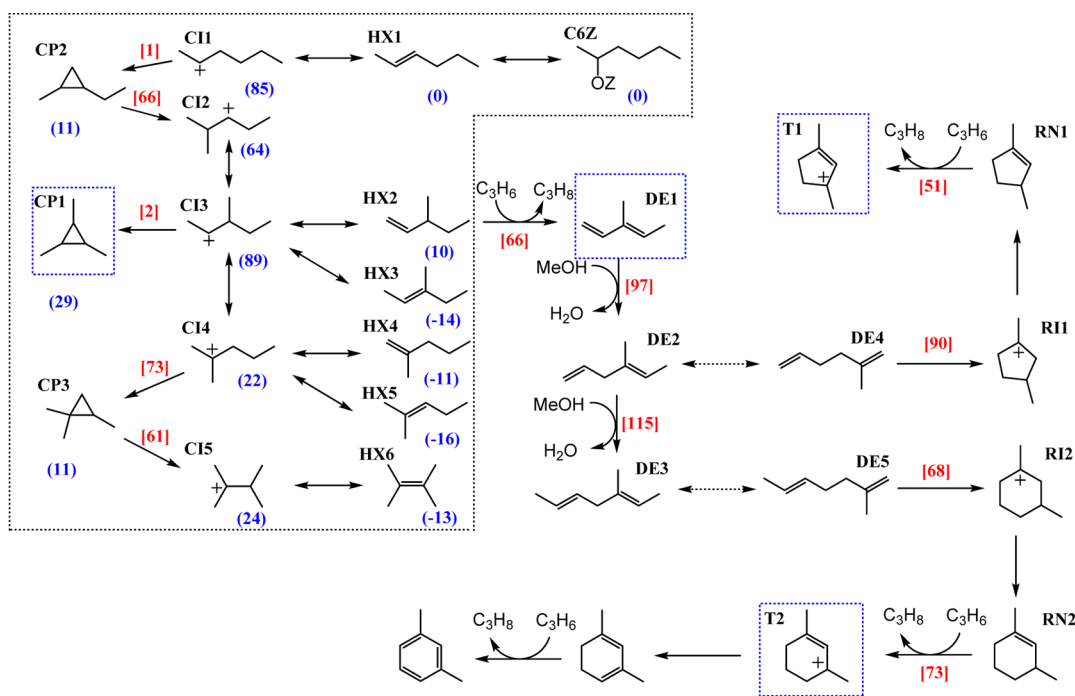
ppm)<sup>48</sup> and trimethylcyclopropane ( $\delta_{13\text{C}} = 9.8$  and  $14.7$  ppm),<sup>48</sup> also occurred in the  $^{13}\text{C}$  MAS NMR spectra.

Upon MTO conversion at  $325\text{ }^\circ\text{C}$ , additional signals appear in the low-field region of  $150\text{--}250$  ppm. To distinguish the central lines and spinning sideband of signals, different spinning rates of 8 and 11 kHz were applied in the  $^{13}\text{C}$  MAS NMR measurements (see Figure S3). Generally, the positions of spinning sidebands are related to the spinning rate of the MAS rotor. After increasing the spinning rate from 8 to 11 kHz, the  $^{13}\text{C}$  NMR signals at 226, 204, and 186 ppm, observed on the used SAPO-34 catalyst after TOS of 15 min at  $325\text{ }^\circ\text{C}$ , were not shifted. This finding implies that the above-mentioned peaks are the central lines of signals and not caused by spinning sidebands. According to the previous studies, the signals at  $\delta_{13\text{C}} = 240\text{--}260$  and  $155$  ppm are attributed to five-ring carbenium ions, such as 1-methyl-2-cyclopentenyl ( $\delta_{13\text{C}} = 46.7, 145.9, 217.1, 259.7$  ppm)<sup>44</sup> and 1,2,3-trimethyl-2-cyclopentenyl cations ( $\delta_{13\text{C}} = 155.3, 247.0$  ppm),<sup>49</sup> as also observed by Goguen et al.<sup>18</sup> after MTO conversion on H-ZSM-5. According to the previous studies, the adsorption of acetone on the Lewis acid sites of zeolites can also give a  $^{13}\text{C}$  MAS NMR signal at about 226 ppm.<sup>47,50,51</sup> However, if a trace amount of acetone can be formed and adsorbed on SAPO-34 zeolite during the MTO conversion, besides the signal at 226 ppm attributed to Lewis acid sites, another strong signal at about 217 ppm attributed to Brønsted acid sites should also occur simultaneously, but the signal at 217 ppm cannot be observed in our case (see Figures 8, 9, and S3). Hence, an assignment of the signal at 226 ppm to adsorbed acetone can be excluded. Based on the reports of Olah et al.,<sup>49</sup> 1,3-dimethyl-2-cyclohexenyl cations ( $\delta_{13\text{C}} = 31.7, 136.8, \text{ and } 226.6$  ppm) in superacidic solvents can give a signal at  $\delta_{13\text{C}} = 226.6$  ppm. Therefore, the weak signal observed at  $\delta_{13\text{C}} = 226$  ppm in the present study can be attributed to six-ring carbenium ions (e.g., polymethylcyclohexenyl cations) which were also found in MTO conversion for the first time. Again, the results of the above-

mentioned  $^{13}\text{C}$  MAS NMR spectra fit well with the  $^1\text{H}$  MAS NMR spectra (vide supra). Upon further increasing the reaction temperature ( $T \geq 350\text{ }^\circ\text{C}$ ), polymethylcyclopentenyl cations (signal at  $240\text{--}260$  ppm) could still be observed even at  $400\text{ }^\circ\text{C}$ , although the polymethylcyclohexenyl cations (signal at 226 ppm) disappears already upon MTO conversion at the relatively low reaction temperature of  $350\text{ }^\circ\text{C}$ . The activation energy barriers for the formation of polymethylcyclopentenyl and polymethylcyclohexenyl cations are discussed below in connection with the presentation of the DFT studies in detail.

Additionally, as shown in Figure 8, right-hand side, all the  $^{13}\text{C}$  NMR signals, due to carbenium ions ( $\delta_{13\text{C}} = 150\text{--}250$  ppm) on the catalysts completely disappear after ammonia loading. Also this finding indicates that a reaction between ammonia and carbenium ions occurs. The new signal at  $\delta_{13\text{C}} = 72$  ppm appearing after the ammonia loading hints to the formation of amines or ammonium substituted organic species and is an additional support for the above-mentioned statement. These results fit well with those of UV-vis and  $^1\text{H}$  MAS NMR spectroscopy (vide supra).

To investigate the fate of the observed intermediates during the early stages of the MTO reaction over H-SAPO-34 catalyst, the samples obtained after different TOS at the reaction temperature of  $325\text{ }^\circ\text{C}$  were also investigated by  $^{13}\text{C}$  MAS NMR spectroscopy. Figure 9 shows the  $^{13}\text{C}$  MAS NMR spectra of the different catalysts before and after ammonia loading. With the increase of TOS, the number of the five-membered ring cations reflected as the intensities of the signals at  $\delta_{13\text{C}} = 240\text{--}250$  and  $154$  ppm increased at first but then gradually decreased (Figure 9, left-hand side). The same trend was also observed for polymethylcyclohexenyl cations ( $\delta_{13\text{C}} = 226$  ppm). In addition, new signals at  $\delta_{13\text{C}} = 187$  and  $204$  ppm appeared after TOS = 15 min. These signals can be attributed to pentamethylbenzenium ion ( $\delta_{13\text{C}} = 206, 190$  ppm).<sup>20</sup> With the further progress of the MTO conversion, the number of polymethylbenzenium cations started to decrease gradually,

Scheme 1. Proposed Reaction Pathway Containing the Observed Intermediates on H-SAPO-34 for the Early Stages of the MTO Conversion<sup>a</sup>

<sup>a</sup>The blue values in parentheses are the relative energies of C6 species. The red values in square brackets are the energy barriers for each elementary step. All values are given in kJ/mol. The abbreviation OZ represents the zeolite framework.

which agrees with the <sup>1</sup>H MAS NMR results (Figure 7). After ammonia loading, all of the above-mentioned signals at  $\delta_{13\text{C}} = 150\text{--}250$  ppm disappeared (Figure 9, right-hand side). This ammonia-induced disappearance of the above-mentioned signals demonstrates that they were caused by carbenium ions.

**3.6. Reaction Mechanism and DFT Studies of MTO Conversion on the H-SAPO-34 Catalysts.** Comparing the catalytic data summarized in Figure 3 and the <sup>13</sup>C MAS NMR results in Figure 9, the number of five- and six-membered cations, reflected by the intensities of their <sup>13</sup>C MAS NMR signals, correlate well with the methanol conversion. The highest methanol conversion was observed at TOS = 15 min, which coincides with the highest concentration of the above-mentioned carbenium ions. It is interesting to note that almost no or only a nondetectable small number of polymethylbenzenium cations occurs during the first 10 min in the MTO reaction over H-SAPO-34 at 325 °C (see Figure 7 and Figure 9), while a methanol conversion already occurred. According to these observations, it can be concluded that polymethylcyclopentenyl and/or polymethylcyclohexenyl cations formed from alkenes play a key role in the early stages of the MTO reaction on H-SAPO-34. Polymethylcyclopentenyl and/or polymethylcyclohexenyl cations formed before the polymethylbenzenium cations could serve as a bridge between olefin-based and aromatic-based cycles at short reaction times. After the formation of aromatics, the aromatic-based cycle may participate in the reaction, which proceeds via the propagation of side alkyl chain and the succedent side-chain elimination to generate light olefins as reaction products.<sup>52–54</sup>

Aiming to rationalize the formation of the intermediates observed on H-SAPO-34 during the early stage of the MTO conversion, we propose a reaction pathway according to an olefin-based cycle as supported by DFT calculations with van

der Waals correction.<sup>55</sup> Olefins with different lengths are probably formed via the methylation of olefins and subsequent cracking steps before the presence of aromatic hydrocarbon pool species. As shown in Scheme 1, hexenes, which can be formed via the methylation of lighter olefins, considered as starting species from which all the other intermediates observed in the present study are evolved. The adsorption energies of hexenes on H-SAPO-34 were calculated to  $-68$  to  $-79$  kJ/mol (Table S1). The protonation of hexenes leads to the formation of C6+ ions (CI1 to CI5) and C6-alkoxide (C6Z), and the latter was used as the energy reference. Due to the inclusion of van der Waals correction, some C6-olefins (HX3 to HX6) are slightly more stable than the secondary C6-alkoxide (C6Z). The characteristics of carbenium ions evidence their stability in the cages and pores of zeolites. These carbenium ions could undergo skeletal isomerization via alkylcyclopropanes intermediates to tune the length of main chains (Figure S4). The CP1 to CP3 alkylcyclopropanes are observed in the experiments, and we found that they are slightly less stable (11–29 kJ/mol) than hexenes.

Propene was selected to be the hydride-acceptor in the hydride transfer step. The hydride transfer between propene and 3-methyl-1-pentene with the energy barrier of 66 kJ/mol leads to the formation of alkadienes. The subsequent methylation of alkadienes propagates the chains. The energy barriers of the methylation were calculated to be 97 and 115 kJ/mol. The cyclization of 2-methyl-1,5-hexadiene (DE4), formed via isomerization from 4-methyl-1,4-hexadiene (DE2), results in the formation of dimethyl-cyclopentanylium (RI1). The subsequent deprotonation and hydride transfer forms the observed intermediate T1 with a five-membered ring. The energy barrier of both cyclization and hydride transfer are less than 95 kJ/mol. Similarly, the intermediate T2 with six-



membered ring can be formed from 2-methyl-1,5-heptadiene via cyclization (68 kJ/mol), deprotonation, and hydride transfer (73 kJ/mol) steps. The repeated deprotonation and hydride transfer steps lead to the formation of methylbenzenes, known as active hydrocarbon pool species in the aromatic-based catalytic cycles. All energy barriers in the proposed pathway are less than 120 kJ/mol, which indicate that these intermediates are stable enough for a spectroscopic observation on H-SAPO-34. All the transition state structures are shown in [Figure S5–S7](#).

On the basis of the proposed reaction pathway, the observability of the polymethylcyclopentenyl (T1) and polymethylcyclohexenyl (T2) cations, which serve as bridges connecting the two parts of the dual-cycle reaction mechanism, can be discussed. According to the reaction pathway presented in Scheme 1, the cyclization and the subsequent hydride transfer are calculated to be more feasible than the growth of higher dienes, and therefore, the latter is the rate-determining step for the formation of T1 or T2. The formation of T1 is slightly preferred compared to T2 (highest energy barrier 97 compared with 115 kJ/mol). Therefore, polymethylcyclopentenyl cations can be earlier observed on H-SAPO-34 catalyst by  $^1\text{H}$  and  $^{13}\text{C}$  MAS NMR spectroscopy than polymethylcyclohexenyl cations.

#### 4. CONCLUSIONS

In summary, several initial species before the formation of polymethylbenzenium cations (e.g., three-ring compounds, dienes, polymethylcyclopentenyl cations, and polymethylcyclohexenyl cations) were directly observed during the MTO conversion on SAPO-34 for the first time, and their evolutions were identified via  $^1\text{H}$  and  $^{13}\text{C}$  MAS NMR spectroscopy. On the basis of the experimental observations, an olefin-based reaction cycle of these species in the initial process of MTO conversion is proposed and proved to be energetically feasible via the theoretical DFT calculations. With the progress of MTO conversion, aromatics are produced and then an aromatics-based cycle may start to participate in the steady-state MTO reaction. The results reported herein not only provide some new experimental findings in the early stages of the MTO conversion but also contribute to the understanding of the induction period in the MTO reaction.

#### ■ ASSOCIATED CONTENT

##### Supporting Information

The following file is available free of charge on the ACS Publications website at DOI: 10.1021/cs5015749.

Simulated structure of H-SAPO-34; in situ UV–vis spectra;  $^{13}\text{C}$  HPDEC MAS NMR spectra; adsorption energies of hexanes; optimized structures and detailed atomic positions of intermediates and transition states ([PDF](#))

#### ■ AUTHOR INFORMATION

##### Corresponding Authors

\*E-mail: michael.hunger@itc.uni-stuttgart.de. Fax: +49-711-685-64081.

\*E-mail: lild@nankai.edu.cn. Fax: +86-22-2350-0341.

##### Notes

The authors declare no competing financial interest.

#### ■ ACKNOWLEDGMENTS

This work was financially supported by the National Natural Science Foundation of China (21303089, 21103231, 21421001), Municipal Natural Science Foundation of Tianjin (14JJCQNJC05700), and China Postdoctoral Science Foundation (2013M530870, 2014T70211). The support from the 111 Project (B12015) and the Ministry of Education of China (IRT13R30, IRT13022) are also acknowledged. Furthermore, M.H. wants to acknowledge the financial support by Deutsche Forschungsgemeinschaft.

#### ■ REFERENCES

- (1) Stöcker, M. In *Zeolite and Catalysis: Synthesis, Reactions and Applications*; Čejka, J., Corma, A., Zones, S., Eds.; Wiley-VCH: Weinheim, 2010; p 687.
- (2) Wang, W.; Hunger, M. *Acc. Chem. Res.* **2008**, *41*, 895–904.
- (3) Olsbye, U.; Svelle, S.; Bjørgen, M.; Beato, P.; Janssens, T. V. W.; Joensen, F.; Bordiga, S.; Lillerud, K. P. *Angew. Chem., Int. Ed.* **2012**, *51*, 5810–5831.
- (4) Hemelsoet, K.; Mynsbrugge, J.; Wispeleere, K.; Waroquier, M.; Speybroeck, V. *ChemPhysChem* **2013**, *14*, 1526–1545.
- (5) Ilias, S.; Bhan, A. *ACS Catal.* **2013**, *3*, 18–31.
- (6) Dai, W. L.; Kong, W. B.; Li, L. D.; Wu, G. J.; Guan, N. J.; Li, N. *ChemCatChem* **2010**, *2*, 1548–1551.
- (7) Dahl, I. M.; Kolboe, S. *Catal. Lett.* **1993**, *20*, 329–336.
- (8) Dahl, I. M.; Kolboe, S. *J. Catal.* **1996**, *161*, 458–464.
- (9) Arstad, B.; Kolboe, S. *J. Am. Chem. Soc.* **2001**, *123*, 8137–8138.
- (10) Song, W. G.; Haw, J. F.; Nicholas, J. B.; Henegha, C. S. *J. Am. Chem. Soc.* **2000**, *122*, 10726–10727.
- (11) Haw, J. F.; Song, W. G.; Marcus, D. M.; Nicholas, J. B. *Acc. Chem. Res.* **2003**, *36*, 317–326.
- (12) Svelle, S.; Joensen, F.; Nerlov, J.; Olsbye, U.; Lillerud, K. P.; Kolboe, S.; Bjørgen, M. *J. Am. Chem. Soc.* **2006**, *128*, 14770–14771.
- (13) Bjørgen, M.; Svelle, S.; Joensen, F.; Nerlov, J.; Kolboe, S.; Bonino, F.; Palumbo, L.; Bordiga, S.; Olsbye, U. *J. Catal.* **2007**, *249*, 195–207.
- (14) Lesthaeghe, D.; Van der Mynsbrugge, J.; Vandichel, M.; Waroquier, M.; Van Speybroeck, V. *ChemCatChem* **2011**, *3*, 208–212.
- (15) Erichsen, M. W.; Svelle, S.; Olsbye, U. *J. Catal.* **2013**, *298*, 94–101.
- (16) Janssens, T. V. W.; Svelle, S.; Olsbye, U. *J. Catal.* **2013**, *308*, 122–130.
- (17) Ilias, S.; Khare, R.; Malek, A.; Bhan, A. *J. Catal.* **2013**, *303*, 135–140.
- (18) Goguen, P.; Xu, T.; Barich, D.; Skloss, T.; Song, W. G.; Wang, Z.; Nicholas, J.; Haw, J. F. *J. Am. Chem. Soc.* **1998**, *120*, 2650–2651.
- (19) Song, W. G.; Nicholas, J. B.; Sassi, A.; Haw, J. F. *Catal. Lett.* **2002**, *81*, 49–53.
- (20) Xu, S. T.; Zheng, A. M.; Wei, Y. X.; Chen, J. R.; Li, J. Z.; Chu, Y. Y.; Zhang, M. Z.; Wang, Q. Y.; Zhou, Y.; Wang, J. B.; Deng, F.; Liu, Z. M. *Angew. Chem., Int. Ed.* **2013**, *52*, 11564–11568.
- (21) Dai, W. L.; Wu, G. J.; Li, L. L.; Guan, N. J.; Hunger, M. *ACS Catal.* **2013**, *3*, 588–596.
- (22) Wang, X.; Dai, W. L.; Wu, G. J.; Li, L. D.; Guan, N. J.; Hunger, M. *Catal. Sci. Technol.* **2014**, *4*, 688–696.
- (23) Wang, C. M.; Brogaard, R. Y.; Weckhuysen, B. M.; Norskov, J. K.; Studt, F. *J. Phys. Chem. Lett.* **2014**, *5*, 1516–1521.
- (24) Blochl, P. E. *Phys. Rev. B* **1994**, *50*, 17953–17979.
- (25) Enkovaara, J.; Rostgaard, C.; Mortensen, J. J.; Chen, J.; Dulak, M.; Ferrighi, L.; Gavnholt, J.; Glinnsvad, C.; Haikola, V.; Hansen, H.; et al. *J. Phys.: Condens. Matter* **2010**, *22*, 253202.
- (26) Wellendorff, J.; Lundgaard, K. T.; Møgelhøj, A.; Petzold, V.; Landis, D. D.; Nørskov, J. K.; Bligaard, T.; Jacobsen, K. W. *Phys. Rev. B* **2012**, *85*, 235149.
- (27) Henkelman, G.; Jonsson, H. *J. Chem. Phys.* **2000**, *113*, 9978–9985.

- (28) Henkelman, G.; Uberuaga, B. P.; Jónsson, H. *J. Chem. Phys.* **2000**, *113*, 9901–9904.
- (29) *Collection of simulated XRD powder patterns for zeolites*, 5th revised ed.; Treacy, M. M. J., Higgins, J. B., Eds.; Elsevier: Amsterdam, 2007.
- (30) Hunger, M.; Brunner, E. In *Molecular Sieves-Science and Technology*, Karge, H. G., Weitkamp, J., Eds.; Springer-Verlag: Berlin, 2004, Vol. 4, pp 201–293.
- (31) Buchholz, A.; Wang, W.; Xu, M. C.; Arnold, A.; Hunger, M. *Microporous Mesoporous Mater.* **2003**, *57*, 157–168.
- (32) Zibrowius, B.; Loeffler, E.; Hunger, M. *Zeolites* **1992**, *12*, 167–174.
- (33) Arstad, B.; Kolboe, S. *Catal. Lett.* **2001**, *77*, 209–212.
- (34) Crews, P.; Rodriguez, J.; Jaspars, M. *Organic Structure Analysis*; Oxford University Press: New York, 1998.
- (35) Deno, N. C.; Bollinger, J.; Friedman, N.; Hafer, K.; Hodge, J. D.; Houser, J. J. *J. Am. Chem. Soc.* **1963**, *85*, 2998–3000.
- (36) Kiricsi, I.; Fçrster, H.; Tasi, G.; Nagy, J. B. *Chem. Rev.* **1999**, *99*, 2085–2114.
- (37) Bjørgen, M.; Bonino, F.; Kolboe, S.; Lillerud, K.-P.; Zecchina, A.; Bordiga, S. *J. Am. Chem. Soc.* **2003**, *125*, 15863–15868.
- (38) Olah, G. A.; Pittman, C. U.; Symons, M. C. R. In *Carbonium Ions I*; Olah, G. A., Schleyer, R.v.R., Eds.; Interscience: New York, 1969; Vol. 1, pp 153–222.
- (39) Dai, W. L.; Scheibe, M.; Guan, N. J.; Li, L. D.; Hunger, M. *ChemCatChem* **2011**, *3*, 1130–1133.
- (40) Jiang, Y. J.; Huang, J.; Dai, W. L.; Hunger, M. *Solid State Nucl. Magn. Reson.* **2011**, *39*, 116–141.
- (41) Bosáček, V.; Ernst, H.; Freude, D.; Mildner, T. *Zeolites* **1997**, *18*, 196–199.
- (42) Hunger, M.; Horvath, T. *J. Am. Chem. Soc.* **1996**, *118*, 12302–12308.
- (43) H NMR Predictor, Product Version 9.08, Advanced Chemistry Development Inc., 2006.
- (44) Olah, G. A.; Liang, G. *J. Am. Chem. Soc.* **1972**, *94*, 6434–6441.
- (45) Dai, W. L.; Scheibe, M.; Li, L. D.; Guan, N. J.; Hunger, M. *J. Phys. Chem. C* **2012**, *116*, 2469–2476.
- (46) Jiang, Y.; Hunger, M.; Wang, W. *J. Am. Chem. Soc.* **2006**, *128*, 11679–11692.
- (47) Dai, W. L.; Wang, X.; Wu, G. J.; Li, L. D.; Guan, N. J.; Hunger, M. *ChemCatChem* **2012**, *4*, 1428–1435.
- (48) C NMR, version 1.1, Advanced Chemistry Development, Inc.: Toronto, Canada, 1995.
- (49) Olah, G. A.; Clifford, P. R.; Halpern, Y.; Johanson, R. G. *J. Am. Chem. Soc.* **1971**, *93*, 4219–4222.
- (50) Song, W. G.; Nicholas, J.; Haw, J. F. *J. Phys. Chem. B* **2001**, *105*, 4317–4323.
- (51) Li, S. H.; Zheng, A. M.; Su, Y. C.; Zhang, H. L.; Chen, L.; Yang, J.; Ye, C. H.; Deng, F. *J. Am. Chem. Soc.* **2007**, *129*, 11161–11171.
- (52) Arstad, B.; Nicholas, J. B.; Haw, J. F. *J. Am. Chem. Soc.* **2004**, *126*, 2991–3001.
- (53) Wang, C. M.; Wang, Y. D.; Xie, Z. K.; Liu, Z. P. *J. Phys. Chem. C* **2009**, *113*, 4584–4591.
- (54) Wang, C. M.; Wang, Y. D.; Xie, Z. K. *Catal. Sci. Technol.* **2014**, *4*, 2631–2638.
- (55) Wang, C. M.; Wang, Y. D.; Xie, Z. K. *J. Catal.* **2013**, *301*, 8–19.